JBIC Journal of Biological Inorganic Chemistry (2018) 23:331–345
https://doi.org/10.1007/s00775-018-1542-z

MINIREVIEW

Inorganic nanoparticles in diagnosis and treatment of breast cancer

Cristina Núñez[1] · Sergio Vázquez Estévez[2] · María del Pilar Chantada[1]

Received: 27 November 2017 / Accepted: 4 February 2018 / Published online: 16 February 2018

Abstract
Nanoparticles are being actively developed for biomolecular profiling of cancer biomarkers, tumor imaging in vivo, and targeted drug delivery. These nanotechnology-based techniques can be applied widely in the management of different malignant diseases, such as breast cancer. Although the number of different types of nanoparticles is increasing rapidly, most can be classified into two major types: particles that contain organic molecules as a major building material (such as dendrimers, micelles, liposomes and carbon nanotubes, and other polymers); and those that use inorganic elements, usually metals, as a core. In particular, inorganic nanoparticles have received increased attention in the recent past as potential diagnostic and therapeutic systems in the field of oncology. This review primarily discusses progress in applications of inorganic nanoparticles for breast cancer imaging and treatment.

Keywords Breast cancer · Gold/magnetic nanoparticles · Quantum dots · Imaging · Therapy

Introduction

Breast cancer is a leading cause of mortality and morbidity for women with 450,000 annual deaths worldwide [1]. Therefore, the diagnosis and cure of BC at early stage is highly necessary to decrease mortality and improve the quality of the lives of patients.

Breast cancer is clinically categorized on the basis of the existence of estrogen receptor (ER), the amplification of HER2/ErbB2 gene and the absence of three nuclear receptors, such as ER, progesterone receptor (PR) and HER2/ErbB2 (Triple Negative). While for the first two groups of breast cancer receptor-specific therapy is applied, chemotherapy remains the mainstay of treatment for triple negative breast cancer (TNBC) [2].

Currently, the best available tool for the early detection of breast cancer is mammography [3]; however up to 20% of new breast cancers are not detected or visible on a mammogram [4]. Magnetic resonance imaging (MRI) and ultrasonography are used in cases of impairment of the latter diagnostic results [5]. Furthermore, it was also found that mammography is better able to detect certain types of breast cancer (such as ductal carcinomas) than other types (such as poor prognosis estrogen receptor (ER)-negative tumors) [6–9].

Continued improvements to detect breast cancer early offer the promise of further reducing the burden of this disease, as breast cancer detected at an earlier stage is much more curable than is metastatic disease.

Recent progress in nanotechnology has shed new light on breast cancer therapy and diagnosis due to the large surface area, high surface reactivity and unique physicochemical properties of these nanostructures [10–12].

The potential of organic nanomaterials for the treatment of breast cancer is well-established and described in detail [13, 14]. In contrast to organic nanoparticles (NPs), inorganic NPs were developed at the end of the last century, and their biomedical applications are relatively recent [15].

All inorganic NPs share a typical core/shell structure. The core can contain metals [iron oxide, gold and quantum dots (QDs)] or organic fluorescent dyes encapsulated in silica. The central core defines the fluorescence, optical, magnetic, and electronic properties of the particle. The shell is usually made of metals or organic polymers that protect the core from chemical interactions with the external environment and/or serves as a substrate for conjugation with

✉ Cristina Núñez
cristina.nunez.gonzalez@sergas.es

[1] Research Unit, Oncology Division, Hospital Universitario Lucus Augusti (HULA), Servicio Galego de Saúde (SERGAS), Lugo, Spain

[2] Oncology Division, Hospital Universitario Lucus Augusti (HULA), Servicio Galego de Saúde (SERGAS), Lugo, Spain

biomolecules, such as antibodies, proteins, and oligonucleotides (see Fig. 1) [16].

During recent years, Núñez et al. have focused on the design of novel nanosystems [17–21] with biological [22] and biomedical applications [23], in particular, breast cancer treatment [24, 25]. Different reviews focused on applications of nanoparticles into predictive oncology of breast cancer [26], but only some of them emphasized on the role of inorganic nanosized objects in the diagnosis and treatment of this malignancy [15]. This review discussed recent advances in the use of a particular type of nanosystems [iron oxide magnetic nanoparticles, semiconductor fluorescent quantum dots and gold nanoparticles (spheres, shells, rods, cages)] in tumor targeting, imaging, photothermal therapy and drug delivery applications in breast cancer.

Superparamagnetic nanoparticles

Superparamagnetic NPs are unique inorganic NPs that were first introduced for biomedical applications in the late 1980s [27]. The core of superparamagnetic NPs consists of metal molecules of nickel, cobalt or iron oxide (Fe_3O_4 magnetite, which is the most commonly used metal). The surface of superparamagnetic NPs can be modified by coating the core in a few atomic layers of organic polymers (dextran [28], starch [29], alginate [30], poly(D,L-lactide-coglycolide) [31], and poly(ethylene–glycol) (PEG) [32]), inorganic metals (gold) or oxides (silica, alumina) [33].

Superparamagnetic NPs can be conjugated with various bioactive ligands and can be used for in vitro and in vivo diagnosis of tumors [34]. To this aim, various methodologies have been developed to synthesize superparamagnetic NPs that are able of distinguishing cancerous tissue from healthy tissue.

Superparamagnetic NPs have been also used successfully for cell labeling, drug delivery, MRI of tumor tissue and vasculature, hyperthermia induction and magnetofection of cancer cells (transfection of vector DNA coupled with magnetic NPs into cells using a magnetic field) [35]. Furthermore, superparamagnetic NPs are also attractive theranostic platforms because of its capability as a drug carrier as well as an MRI contrast (see Table 1).

Magnetic resonance imaging (MRI) is one non-invasive medical diagnostic technique. The MR images of normal and abnormal tissues are difficult to differentiate; therefore, specific exogenous contrast agents are used in order to increase the contrast and obtain higher resolution and sensitivity.

The size and the large surface area of the metal NPs with superparamagnetic phenomena provide a detectable magnetic resonance (MR) signal. In particular, superparamagnetic iron oxide nanoparticles (SPIONs) have been extensively studied as T_2 contrast agents in magnetic resonance imaging (MRI). This is due to the negative contrast (darkness) in phantom images that can be enhanced by T_2 relaxivity of water protons.

Several breast cancer cell markers receptors such as gastrin-releasing peptide (GRP), integrin $\alpha_v\beta_3$, transferrin (Tf), human epidermal growth factor receptor-2 (Her2), folic/folate, CD44 and urokinase-type plasminogen activator (uPA) have been used for targeting of magnetic

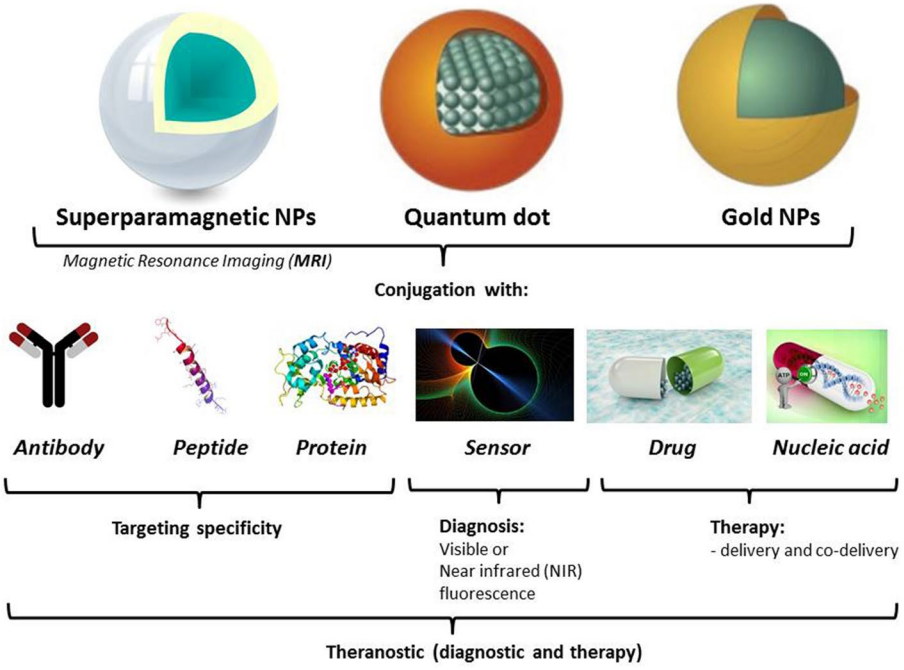

Fig. 1 Basic structure and functional ligands of inorganic nanoparticles used in breast cancer diagnosis and therapy

Table 1 Examples of active-targeting magnetic nanoplatforms evaluated in breast cancer imaging and therapy

Magnetic nanoprobe	Size	Targeting strategy	Method	References
SPIONs coated with dextran (DSPIONs)	6.0 ± 0.5 nm	Bombesin (BBN)	MRI in vitro and in vivo	[38]
Dual-targeting poly(ethylene glycol)-poly(ε-caprolactone) (PEG-b-PCL) micelles encapsulating SPIONs	39.9 ± 1.9 nm	Cyclic form of arginine-glycine-aspartic acid peptides (cRGD) and the single chain HER-2 antibody fragment (scFv-ErbB)	MRI in vivo	[40]
SPION-encapsulated magnetoliposomes	120–129 nm	Biotin	MRI in vivo	[41]
Ultrasmall superparamagnetic iron oxide nanoparticles (USPIONs)	36 nm	Human transferrin	MRI in vivo	[42]
SPIONs functionalized with dextran	3.5 ± 0.3 nm	Anti-HER2 antibody (Herceptin)	MRI in vitro and in vivo	[43]
Magnetic iron oxide nanocrystals	14 nm	Anti-HER2 antibody (Herceptin) and a fluorescent dye-labeled secondary antibody of human IgG	MRI in vitro and in vivo	[44]
SPIONs coated with chitosan and PEG labeled with a fluorescent dye (Alexa Fluor 647 or Oregon Green 488)	40–47 nm	Monoclonal antibody (mAb) against the Neu receptor (NP-neu)	MRI in vitro and in vivo	[45]
Iron oxide nanoparticles coated with dextran	100 nm	Anti-HER2 antibody (Herceptin)	Magnetic hyperthermia in vitro (35 °C for 20 min; H ~ 36 kA/m, $f = 163$ kHz)	[46]
SPION coated with poly(ethylene glycol (PEG)	30.2 nm (~ 274 molecules of paclitaxel per particle)	Anti-HER2 antibody (Herceptin)	MRI and drug delivery [paclitaxel (PTX)] in vitro and in vivo	[47]
Polyethylenimine (PEI)-coated hollow manganese oxide nanoparticles	20 nm	Anti-HER2 antibody (Herceptin)	MRI and gene delivery (siRNA) in vitro	[48]
Iron oxide magnetic nanoparticles	93 nm (~ 20 µmol gemcitabine per g Fe)	Anti-CD44 antibody	MRI and drug delivery [gemcitabine (GEM)] in vitro and in vivo	[49]
SPIONs were initially coated with covalently-bound bifunctional PEG	9–11 nm	Folic acid	MRI in vitro	[50]
Silica-coated manganese oxide nanoparticle covalently conjugated with Rhodamine B isothiocyanate (RBITC)	~ 35 nm	Folate (FA)	MRI and FI (fluorescence imaging) in vitro and in vivo	[51]
SPIONs functionalized with APTES [(3-aminopropyl) triethoxysilane] and polyethylene glycol (PEG)	~ 13 nm	Folic acid	Drug delivery [carboxylated quercetin (CQ)]	[52, 53]
Iron oxide nanoparticles loaded with the fluorescent Cy5 dye	5–10 nm	Urokinase-type plasminogen activator (uPA)	MRI, optical imaging and drug delivery [doxorubicin (DOX)] in vitro and in vivo	[54, 55]
Fe_3O_4-encapsulated block copolymer containing methoxy poly(ethylene glycol) (PEG) and poly(β-amino ester) (PAE) conjugating with fluorescent dye Sulforhodamine 101	87 ± 3 nm	–	FI-MRI dual-modality in vitro	[56]

Table 1 (continued)

Magnetic nanoprobe	Size	Targeting strategy	Method	References
Polyethylene glycol-coated ultrasmall gadolinium oxide (PEG-Gd_2O_3)/aptamer-Ag nanoclusters (NCs)	20 nm	–	FI-MRI dual-modality in vitro	[57]
Iron oxide NPs modified with a self-assembled monolayer (SAM) of (3-aminopropyl)trimethoxysilane	10 nm	–	MRI and drug delivery [methotrexate (MTX)] in vitro	[58]
Superparamagnetic poly(lactic-*co*-glycolic acid) microcapsules (Fe_3O_4/PLGA)	885.6 nm	–	Ultrasound/MRI dual-modality in vitro and in vivo	[59]
Double emulsion nanocapsules (DENCs) stabilized by a single-component poly(vinyl alcohol) (PVA) with magnetic nanoparticles	174 ± 13 nm	Anti-HER2 antibody (Herceptin)	Drug co-delivery (doxorubicin (DOX) and hydrophobic [paclitaxel (PTX)] in vitro and in vivo	[63]
Iron oxide superparamagnetic iron oxide nanocrystals within folate-functionalized lipid nanoparticles (LNPs)	170 nm	Folate (FA)	MRI and drug delivery [paclitaxel (PTX)] in vitro and in vivo	[64]

nanoparticles to breast cancer tissue for imaging and diagnostic applications.

Peptide-conjugated SPIONs have shown great potential as contrast agents for in vivo tumor detection using MRI. In particular, Bombesin (BBN) and its human counterpart, gastrin-releasing peptide (GRP) play an important role in cancer growth [36]. It was found that GRP receptors are overexpressed in many cancers, including breast cancer [37]. SPIONs coated with dextran (DSPIONs) conjugated with bombesin (BBN) were developed to produce a targeting contrast agent (DSPION-BBN) for the detection of breast using MRI [38]. It was found a good targeting ability of DSPION-BBN for binding T47D breast cancer cells overexpressing gastrin-releasing peptide (GRP) receptors. Furthermore, DSPION-BBN possessed good diagnostic capability as a contrast agent, with appropriate signal reduction in T_2^*-weighted color map MR imaging in mice with BC.

Integrins are heterodimeric transmembrane glycoproteins that act as receptors for molecules of the extracellular matrix (ECM). Integrin $\alpha_v\beta_3$ is of particular interest as an in vivo imaging target, since it is known to be involved in the process of tumor development, angiogenesis, and metastases, and can thus be found on angiogenic vessels in malignant tumors. Moreover, integrin $\alpha_v\beta_3$ show a high binding affinity for arginine-glycine-aspartic acid (RGD) peptides, which naturally occur in ligands specific to integrin receptors. Consequently, RGD peptides have been extensively used as targeting moieties for functionalization of different NP systems, including SPIONs [39].

Following this strategy, Gong et al. [40] fabricated dual-targeting micelles encapsulating SPIONs from the amphiphilic block copolymer poly(ethylene glycol)-poly(ε-caprolactone) (PEG-b-PCL) conjugated at the distal ends of the PEG block with the cyclic form of RGD peptides (cRGD) and the single chain HER-2 antibody fragment (scFv-ErbB) for human epidermal growth factor receptor-2 overexpressed in breast tumor cells. The efficiency of fabricated contrast agent was assessed on an animal model produced by subcutaneous injection of BT474 cells into the BALB/c-un female nude mice with a 1.5 T clinical MRI scanner. It was found that the magnetic system delivered by tail vein injection decreased the T_2 signal intensity of the tumor in animals to a higher extent than single ligand-targeted and non-targeted magnetic micelles.

PEG-modified and SPION-encapsulated magnetoliposomes with biotin were also prepared to target integrin $\alpha_v\beta_3$ for breast cancer imaging [41]. In a guided 3-step targeting approach, biotinylated anti-$\alpha_v\beta_3$ mAbs were intravenously injected into mice bearing MDA-MB-435S breast tumors, followed by injection of avidin/streptavidin and finally, injection of the biotinylated magnetoliposomes. Fluorescence immunohistochemistry and Prussian blue staining were employed to determine the specificity of $\alpha_v\beta_3$ targeting.

The 3-step pre-targeting approach enhanced the MRI contrast to a larger extent compared with no targeting (7.0% of the tumor area vs. 2.0%), and the targeted magnetoliposomes were shown to colocalize with neovasculature.

Human transferrin (Tf) was covalently coupled to ultrasmall superparamagnetic iron oxide nanoparticles (USPIONs) for in vivo imaging of SMT/2A tumor-bearing rats (rat mammary carcinoma) [42]. It was found that with a half-life of 17 min in normal rats, the conjugates could reduce the MRI signal of the tumor by 40% (range 25–55%) 150 min after injection, and this signal reduction could be maintained for at least 8 h. By comparison, the identical parent USPIONs or those labeled with human serum albumin could only induce a 10% reduction in tumor signal over time.

Her2/Neu receptors are among the most specific markers in targeting, staging, and treatment of breast cancer. To validate the targeting specificity, SPIONs functionalized with dextran and anti-HER2 antibodies (Herceptin) were synthesized and their MR signal was tested on four different breast cancer cell lines: BT-474, SKBR-3, MDA MB-231, and MCF-7 [43]. In fact, MR signal was greater in cell lines with higher HER2/neu expression; however, even cell lines with low HER2/neu expression levels could be adequately detected. Upon intravenous injection of these NPs into mice bearing breast tumor allografts, a 45% drop in MR enhancement was seen in T2-weighted MR images, which indicated the high accumulation of NPs within the tumor site.

Huh et al. [44] synthesized magnetic iron oxide nanocrystals conjugated to anti-HER2 antibodies (Herceptin) and also with a fluorescent dye-labeled secondary antibody of human IgG, allowing them to be used both for in vitro and ex vivo optical detection of cancer as well as for in vivo MRI. In a similar way, Kievit et al. [45] coated 8 nm SPIONs with a chitosan/PEG copolymer, labeled them with a fluorescent dye (Alexa Fluor 647 for in vivo or Oregon Green 488 for in vitro detection), and further functionalized them with a monoclonal antibody against the neu receptor (NP-neu). The Neu-functionalized NPs were highly internalized by Neu-expressing mouse mammary carcinoma (MMC) cells, and specificity to the Neu antigen was demonstrated by reversal of the internalization in the presence of free Neu antibody. It was found that the bioconjugates could accurately label breast tumors with MRI and optical dual modality.

Magnetic hyperthermia (MH) is one form of thermal therapy in which magnetic nanoparticles produce heat in the presence of an alternating magnetic field. Multifunctional SPIONs have been used in magnetic hyperthermia (MH) treatment of cancer. Zhang et al. [46] evaluated the capacity of anti-HER2-iron oxide nanoparticles coated with dextran to selectively kill HER2-positive breast cancer SKBr3 cells under an alternating magnetic field exposure The accumulation of anti-HER2-iron oxide nanoparticles was observed in SKBr3 but not in HER2-negative normal human mammary epithelial cells (HMEC). Due to the active-targeting, a significant increase in nanoparticle retention (up to 30%) was observed in HER2-positive cells compared to non-targeted particles, which led to a specific and more pronounced cell death effect after MH treatment.

It was found that anti-HER2 targeted-PEGylated SPIONs loaded with paclitaxel presented a 2.5-fold increased uptake in cells overexpressing HER-2 compared to cells with low levels of this receptor in a human HER2/neu+ SK-BR-3 breast cancer xenograft mouse model as well as a selective and increased breast cancer cell death in vitro compared to free paclitaxel [47]. The same study also showed reduced paclitaxel toxicity for non-target cells when the drug is conjugated with nanoparticles compared to the drug free.

Bae et al. [48] developed a novel multi-functional agents nanosystem that potentially could be employed for cancer therapy using therapeutic siRNA and MRI-based diagnosis. To this aim, they synthesized PEI-coated hollow manganese oxide nanoparticles for cancer targeted siRNA delivery functionalized with anti-HER2 antibodies (Herceptin). Herceptin-mediated targeting increased intracellular delivery and the therapeutic effects of VEGF siRNA against the cancer cells. This system efficiently generated strong positive T1 contrast on the MR image and also delivered therapeutic siRNA into human breast cancer cells.

Aires et al. [49] developed a specific drug delivery system based on iron oxide nanoparticles conjugated with the antibody (anti-CD44) and gemcitabine (GEM) for CD44+ breast cancer cells therapeutics. The treatment with anti-CD44-GEM-iron oxide nanoparticles (4 μM of GEM) decreased significantly MDA-MB-231 breast cancer cells viability (CD44+) in vitro compared to non-targeted GEM-iron oxide nanoparticles or lower doses of drug free (0.4 and 1 μM). However, no difference in cell viability was observed when the free GEM was delivered at the same concentration as in the nanoplatform (4 μM of GEM).

In a study developed by Sun et al. [50], SPIONs were initially coated with covalently-bound bifunctional PEG and subsequently conjugated with folic acid. The NPs were shown to preferentially target the folate receptors (FR) overexpressing HeLa cells and not the non-FR expressing MG-63 osteosarcoma cells. The uptake of folic acid-functionalized NPs in HeLa cells was 12-fold higher than non-targeted NPs after 4 h of incubation. It was found that the functionalized NPs caused a significant contrast enhancement in HeLa cells compared to MG-63 cells in vitro. Similarly, an excellent platform for both MRI and fluorescence imaging (FI) that also specifically target cancer cells overexpressed folate (FA) receptors were developed by Shi and Yang group [51]. They prepared monodisperse silica-coated manganese oxide nanoparticle (NPs) covalently conjugated with Rhodamine B isothiocyanate (RBITC) and folate (FA) on the surface.

Superparamagnetic iron oxide nanosystems (SPION) functionalized with APTES [(3-aminopropyl) triethoxysilane] and polyethylene glycol (PEG), and conjugated with folic acid (FA) were also employed as anticancer drugs carriers of carboxylate quercetin (CQ) [52, 53]. Importantly, this newly synthesized SPION@APTES@FAPEG@CQ nanosystem showed great potential for the treatment of brain adenocarcinoma [52] and could be used for the delivery of quercetin to cervical and breast cancer cells [53].

A multi-modal system composed of iron oxide nanoparticles coated with the amino-terminal fragments of urokinase-type plasminogen activator (uPA) (8–10 molecules per particle) and loaded with the fluorescent Cy5 dye and a therapeutic agent [fluorescent drug doxorubicin (Dox)] was developed for combined MRI and optical imaging of breast cancer cells [54]. In vitro data indicate that uPAR-targeted SPIONs-Dox delivered high levels of Dox into 4T1 and MDA-MB 231 cells and produce a strong inhibitory effect on cell growth when compared to cells treated with free Dox or nontargeted SPIONs-Dox. The ability of targeted therapy and MRI of nanoparticle-drug delivery following systemic delivery of uPAR-targeted IONP-Dox theranostic IONPs were demonstrated in 4T1 mouse mammary tumor model [55].

Other example of fluorescence imaging (FI)-MRI dual-modality imaging nanoprobe was recently reported [56]. It was based on a Fe_3O_4-encapsulated block copolymer containing methoxy poly(ethylene glycol) (PEG) (as a hydrophilic segment) and poly(β-amino ester) (PAE) (with ionizable tertiary amine groups as a pH-responsive segment) conjugating with fluorescent dye Sulforhodamine 101. The nanoprobes could be internalized into breast cancer cells, which were probably used in biomedical diagnosis fields. Other similar nanoprobe based on polyethylene glycol-coated ultrasmall gadolinium oxide (PEG-Gd_2O_3)/aptamer-Ag nanoclusters (NCs) was employed for the effectively tracked of MCF-7 tumor cells by FI and MRI in vitro [57].

For simultaneous MR imaging and drug delivery to breast cancer, iron oxide NPs modified with a self-assembled monolayer (SAM) of (3-aminopropyl)trimethoxysilane and covalently bound with MTX were synthesized [58]. The SAM-modified NPs were conjugated with methotrexate (MTX) through an amide bond, such that MTX could be cleaved from the NPs in the low pH environment of lysosomes after cellular uptake. In human MCF-7 and HeLa cancer cell lines, MTX release was monitored by UV absorbance (at 304 nm) under conditions that simulated lysosomal pH and protease levels. Finally, cells expressing the FR were shown to internalize the NP to a higher extent than non-FR expressing cells.

Sun et al. [59] prepared superparamagnetic poly(lactic-*co*-glycolic acid) microcapsules (Fe_3O_4/PLGA). Ultrasound/MRI dual-modality biological imaging in vitro and in vivo of breast cancer were developed. The bioconjugates presented a good ultrasound imaging and MRI imaging capability, providing an alternative strategy for highly efficient imaging guided non-invasive breast cancer therapy. Other research groups also obtained similar good results [60–62].

Magnetic nanoparticles were also used for the simultaneously co-delivery of two small molecules such as drugs, DNA or RNA [25]. Following this idea, Chiang et al. [63] fabricated trastuzumab-conjugated pH-sensitive double emulsion nanocapsules (DENCs) for simultaneously targeted delivery of hydrophilic doxorubicin (Dox) and hydrophobic paclitaxel (PTX). Confocal images revealed significantly elevated cellular uptake of trastuzumab-conjugated DENCs in HER-2 overexpressing SkBr3 cells. It is important to mention that an intravenous injection of this co-delivery system followed by magnetic targeting (MT) chemotherapy suppressed cancer growth in vivo more efficiently than the delivery of either PTX or DOX alone.

More recently, Lee [64] co-encapsulated iron oxide superparamagnetic iron oxide nanocrystals (6.8 wt%, 11 nm in diameter) and the poorly soluble anti-cancer drug paclitaxel (4.7 wt%) within folate-functionalized lipid nanoparticles (LNPs). This nanosystem enabled both, the targeted detection of MCF-7 (human breast adenocarcinoma expressing folate receptors) in T_2-weighted magnetic resonance images, and the efficient intracellular delivery of paclitaxel. Furthermore, it was also showed in a mouse tumor model that the low-density lipoprotein-mimetic LNPs can be an effective theranostic platform with excellent biocompatibility for the tumor-targeted co-delivery of various anticancer therapeutic and imaging agents.

Quantum dots

Typical quantum dots (QDs) have a core/shell structure consisting of molecules of hard metals, such as technetium, cadmium selenide, zinc, indium or tantalum [65]. The most commonly used, commercially available QDs contain a cadmium selenide core covered with a zinc-sulfide shell. The core–shell complex is generally encapsulated in a coordinating ligand and an amphiphilic polymer [66].

Owing to their unique optical properties, QDs have been developed as fluorescent probes for biomedical applications [67]. Particularly, QDs have a narrow emission spectrum but a size-dependent tunable emission wavelength ranging from visible to near-infrared (NIR) light.

These properties makes QDs-based imaging widely applicable for tissue and in vivo BC studies (see Table 2). Particularly, QDs were an useful tool to observe the four initial steps of cancer metastasis: cancer cells far from blood vessels in tumor, near the vessel, in the bloodstream,

Table 2 Examples of active-targeting quantum dots evaluated in breast cancer imaging and therapy

Nanoprobe	Size	Targeting strategy	Method	References
Quantum dots (QDs)	–	Anti-HER2 antibody (Herceptin)	FI in vitro and in vivo	[70]
Quantum dots and targeting proteins (QD-4D5scFv) and quantum dots coated with polyethylene glycol (PEG) (QD-PEG)	–	Anti-HER2/neu scFv antibodies	FI in vivo	[72]
Quantum dots (QDs)	–	Anti-HER2 (Herceptin) and anti-estrogen receptor (ER) antibodies	Multiplexed FI in vitro	[74]
Quantum dots (QDs)	–	Anti-HER2 (Herceptin)	FI in vitro	[75]
Quantum dots (QDs)	–	Anti-HER2 (Herceptin), anti-estrogen receptor (ER), anti-progesterone receptor (PR), anti-EGFR and anti-mTOR antibodies	Multiplexed FI in vitro	[76]
Quantum dots (QDs)	–	Immunoglobulin G (IgG) and streptavidin	Multiplexed FI in vitro	[77]
Iron oxides (IOs) and quantum dots (QDs) formulated in poly(lactic acid)-D-alpha-tocopheryl polyethylene glycol 1000 succinate nanoparticles (PLA-TPGS NPs)	325.8 ± 5.2 nm	–	MRI and FI in vivo	[78]
Core/shell nanoprobe containing ferric oxide (core), visible-fluorescent QDs (inner shell), and NIR QDs (outer shell)	150 nm	Anti-HER2 (Herceptin) antibody	MRI and FI in vivo	[79]
A complex containing QDs and iron oxide	60–70 nm	–	MRI, near infra-red (NIR)-FI and drug delivery [doxorubicin (DOX)] in vivo	[80]
Quantum dots (QDs)	–	Monoclonal anti-HER2 antibody (trastuzumab)	FI in vivo	[81]
Hydrophilic 2-mercaptosuccinic acid (MSA)-capped QDs encapsulated in the core of the polyethylene glycol-poly(D,L-lactic-*co*-glycolic acid) (PEG-PLGA) nanopolymersomes	140–170 nm (~ 40 μg of DOX per milligram of nanoparticle)	Folate	FI and drug delivery [doxorubicin (DOX)] in vivo	[82]
Nanometer-sized chitosan NPs doped with fluorescent quantum dots (QDs)	60 nm	Anti-HER2 (Herceptin) antibody	FI and gene delivery (HER2 siRNA) in vitro	[83]
Quantum dots (QDs) with two proton-absorbing chemical groups on the surface (carboxylic acid and tertiary amine)	17 nm	–	FI and gene delivery (siRNA) in vitro	[84]

and adherent to the inner vascular surface in the normal tissues near tumor [68].

In this way, anti-HER2-antibody labelled QDs have been also reported to visualize HER2 in human breast adenocarcinoma cell line over-expressing HER2 [69] and these functionalized QDs were also used effectively as only in vivo method for HER2 detection [70]. Furthermore, this QDs immunofluorescence technology was used to quantify HER2 expression in BC [71].

Following this methodology, Balalaeva et al. [72] developed QDs coated with polyethyleneglycol and QDs bound with anti-HER2/neu scFv antibodies (QD-4D5scFv). HER2/neu positive breast cancer tumor xenografts in nude mice were used as a model. It was shown that both bioinert and tumor-targeted QD probes can be successfully applied for visualization of the tumor using in vivo imaging method, but fluorescent signal of QD-4D5scFv in tumors was considerably stronger than that of QD-PEG.

The development of QDs-based multiplexed imaging also showed enormous potentials for in situ multiplexed imaging to simultaneously reveal the interactions of different molecules [73]. In order to understand the evolutionary process of BC heterogeneity, QDs-based quantitative and in situ multiplexed imaging on human epidermal growth factor receptor-2 (HER2) and estrogen receptor (ER) of BC tissues were developed [74]. Furthermore, QDs-based multiplexed imaging on HER2 and IV collagen was also determined. It was demonstrated the invasive behaviors of BC by progressive degradation and destruction IV collagen with the increase of HER2 expression level in BC tissue, especially at the invasion edge [75].

In this way, Yezhelyev et al. [76] developed a quantum dot-based assay that allows quantitative detection of oestrogen receptor (ER), progesterone receptor (PR), and ERBB2 in paraffin-embedded human breast-cancer cell. They demonstrated the feasibility of multiplexed labeling. QDs emitting at 525, 565, 605, 655 and 705 nm were directly conjugated to primary Abs against HER2 (QD-HER2), ER (QD-ER), PR (QD-PR), EGFR (QD-EGFR) and mTOR (QD-mTOR). The multicolor bioconjugates were used for simultaneous detection of the five clinically significant tumor markers in breast cancer cells with different expression levels of the five protein markers: MCF-7 and BT-474. Using multispectral confocal microscope spectrally separated QD fluorescence was clearly visible in both cell lines.

Other example of multiple target detection was recently reported Wu et al. [77]. QDs were linked with immunoglobulin G (IgG) and streptavidin for the simultaneous labelling of HER 2 on both the surface of the cells and in the nucleus. They detected two cellular targets at a single excitation wavelength and found different colors of quantum dots. This experiment showed that QDs with different sizes could be used both to highlight and distinguish different subcellular structures with different colors.

A multimodality nanoprobe containing QDs and magnetic iron oxides was developed by Tan et al. [78] to perform dual-modal image of QDs and MRI in BC bearing mice. Subsequently, a multilayered, core/shell nanoprobe containing ferric oxide (core), visible-fluorescent QDs (inner shell), and NIR QDs (outer shell) was fabricated by Q. Ma et al. [79] to conduct in vivo multimodality imaging. With mean size of 150 nm, dual fluorescence at 600 and 750 nm and competent magnetic property, this nanoprobe were conjugated with anti-HER2 antibody to achieve both NIR imaging and targeted MRI of BC tumor in nude mice.

A complex containing QDs, iron oxide, and doxorubicin was synthesized by Park et al. [80] to perform MRI, QDs-based imaging, and therapy on BC-bearing nude mice. In addition, complex of QDs and the monoclonal anti-HER2 antibody (Trastuzumab) can achieve high-resolution 3-dimensional target imaging in BC-bearing mice [81]. Besides target imaging, the complex containing QDs and trastuzumab could also have therapeutic effect on BC.

More recently, Alibolandi et al. [82] encapsulated hydrophobic doxorubicin (DOX) and hydrophilic 2-mercaptosuccinic acid (MSA)-capped QDs in the bilayer and core of the polyethylene glycol-poly(D,L-lactic-*co*-glycolic acid) (PEG-PLGA) nanopolymersomes, respectively. To achieve active cancer targeting in vitro and in vivo, QDs and DOX-encapsulated nanopolymersomes (NPM) were conjugated with folate for folate-binding protein receptor-guided delivery. Particularly, it was observed that the folate receptor-targeted QDs encapsulated NPM accumulate at tumor sites 6 h following intravenous injection in BALB/c mice bearing 4T1 breast adenocarcinoma. In vivo experiments illustrated a high potential of the prepared targeted theranostic nanoplatform in the treatment and imaging of breast cancer.

Although conventional organic fluorophores have been used to track the delivery of short-interfering RNA (siRNA) in vitro, they do not match the superior optical properties possessed by QDs. In this way, nanometer-sized chitosan NPs doped with fluorescent quantum dots (QDs) were synthesized and targeted delivery of HER2 siRNA to HER2-overexpressing SKBR3 breast cancer cells was shown to be specific with chitosan/QDs NP surface labeled with HER2 antibody [83].

Multifunctional nanoparticles for highly effective siRNA delivery and imaging by balancing two proton-absorbing (that is, proton sponge) chemical groups (carboxylic acid and tertiary amine) on the QD surface were also developed [84]. With a balanced composition of tertiary amine and carboxylic acid groups, these nanoprobes were designed to address longstanding barriers in siRNA delivery such as endosomal release, carrier unpacking, cellular penetration, and intracellular transport. It was found a reduction in

cellular toxicity by 5 to 6-fold and a simultaneous dramatic improvement in gene silencing efficiency by 10 to 20-fold, when compared directly with existing transfection agents for MDA-MB-231 cells. The QD-siRNA nanoprobes were also dual-modality electron-microscopy and optical probes, allowing ultrastructural localization of QDs during delivery and transfection and real-time tracking.

The precise excision of tumor with minimal damage on normal tissues could be promoted by targeted removal of tumor. It was found that under the guidance of NIR QDs imaging on xenografted tumor, targeted removal of subcutaneous tumor was successfully performed [85]. Moreover, with the development of fluorescence-mediated tomography, the in vivo fluorescence imaging depth could reach as deep as 10 cm [86], which may be useful to guide intraoperative surgery for deep BC mass in the near future.

On the other hand, the heat produced by QDs when excited by laser irradiation can be used for selected destruction of deep tumor and highly sensitive imaging. QDs embedded in quantum well was applied by SalmanOgli et al. [87] to enhance sensitivity of thermal detection on small tumor based on the difference of temperature between tumor and normal tissue by computational model-based difference methods.

Gold nanoparticles

Gold nanoparticles (GNPs) have been used in nanobiotechnology over the last four decades as immunocytochemical probes and biological tags [88]. Similar to other inorganic NPs, gold NPs can be linked to targeting ligands and used for selective antitumor therapy [89]. Additionally, the ability to absorb light by gold NPs has been adopted for the optical detection of tumor antigens with simultaneous local tumor thermotherapy (see Table 3) [90].

Gold nanoparticles have been actively used in various visualization and bioimaging methods to identify chemical and biological agents [91, 92]. For example, GNPs functionalized with PEG and coumarin were shown to be effectively internalized by the human breast carcinoma cells without causing any toxicity [93]. However, Núñez et al. [24] have recently reported the synthesis of modified gold nanoparticles having functional quinoline molecules (GNPs@L) that induced apoptosis in MCF-7 cancer cells. It was observed that GNPs@L induced half maximal cytotoxicity (IC_{50}) at 6.25 ± 1.85 and 5.22 ± 1.29 μg/ml concentrations at 24 and 72 h, respectively. It was also observed that GNPs@L increased the percentage of apoptosis at IC_{50} dose, from 5.87% in control cells to 22.31% in cells treated with GNPs@L.

Futhermore, in vitro confocal images of MCF-7 cells incubated with 15 μg/ml of GNPs@L for 3 h. showed that gold nanoparticles were internalized by the MCF-7 cells. Nanoparticles were located mainly in the cytoplasm, as clusters of many GNPs with 1–2 μm in size (green arrows) (see Fig. 2). The mechanism of entrance of the gold nanoparticles in the cells was via the receptor-mediated endocytosis pathway (RME) where a ligand binds onto a receptor on the cell's surface and enters the cell when the membrane invaginates.

Recently, gold nanoparticles decorated with ruthenium(II) metal complexes were also reported as DNA targeting supramolecular structures and luminescent cellular imaging agents [94, 95]. Moreover, protein-sized bioorthogonal nanozymes were developed through the encapsulation of hydrophobic transition metal catalysts into the monolayer of water-soluble GNPs. These nanosystems were used for the cellular delivery of catalysts and the activation of caged cytotoxic molecules [96].

Bioconjugated gold nanorods (GNRs) have been also employed as probes for imaging. For example, a mouse monoclonal antibody specific to human epidermal growth factor receptor 2 (HER2), was conjugated to either GNPs or nanorods to be used for biomedical imaging of SKBR3 breast carcinoma cells [97]. Herceptin-polyethylene glycol(PEG)-gold nanorods were employed for in vivo targeting to breast cancer in nude mice model for breast carcinoma [98].

On the other hand, passive as well as active targeting of gold nanoparticles have been investigated for in vivo photoacoustic tomography (PAT) imaging of tumors, which combines high optical contrast and ultrasound resolution. In this way, after 6 h post-injection, the accumulation of gold nanostars conjugated with cyclic RGD peptides (RGD-gold nanostars) in tumor vessels led to a significant 3.5-fold increase in the photoacoustic signal compared to nontargeted PEG-gold nanostars [99]. Additionally, targeted golden carbon nanotubes (GNTs) conjugated with folic acid were used for a molecular detection of circulating breast tumor cells for photoacoustic imaging in vivo [100]. This approach provided a significant sensitivity improvement (up to 103-fold gain) in circulating tumor cell (CTC) detection, important biomarkers for breast cancer prognosis and therapy prediction [101].

Nanoscale noble metals such as gold with different shapes (cages, shells, stars, rods) have shown a tremendous potential as photothermal agents in cancer photothermal therapy (PTT). Their tunable optical properties that can be carefully optimized to enhance the light absorption from an excitation source (e.g. near infrared (NIR) lasers that can penetrate tissue somewhat) and convert it into heat, making gold nanoparticles ideal for thermal therapy applications [102]. Since relatively lower energies are needed, heating leads to tumor ablation in a minimally invasive way.

Table 3 Examples of active-targeting gold nanoplatforms evaluated in breast cancer imaging and therapy

Nanoprobe	Size	Targeting strategy	Method	References
Gold nanoparticles functionalized with a quinoline ligand (GNPs@L)	2.9 ± 1.2 nm	–	FI and cytotoxicity in vitro	[24]
Gold nanorods (GNRs)	3.6 ± 0.6 nm	Anti-HER2 (Herceptin) antibody	Optical imaging in vitro	[97]
Polyethylene glycol-gold nanorods (PEG-GNRs)	–	Anti-HER2 (Herceptin) antibody	Optical imaging in vivo	[98]
Gold nanostars	55 ± 5 nm	Cyclic RGD peptides	Photoacoustic tomography (PAT) in vivo	[99]
Golden carbon nanotubes (GNTs)	–	Folic acid (FA)	Photoacoustic detection in vitro and in vivo	[100]
Gold nanocages (GNCs)	45 nm	Anti-HER2 (Herceptin) antibody	Photothermal therapy (PTT) in vitro	[103, 104]
Silica-gold nanoshells (GNShs)	75 nm	Anti-HER2 (Herceptin) antibody	Photothermal ablation in vitro	[106]
PEGylated gold nanostars (PEG-GNSs)	60 nm	–	Photothermal ablation in vitro and in vivo	[108]
TAT-peptide functionalized gold nanostars (TAT-GNSs)	–	–	Photothermolysis in vitro	[109]
Polyethylene glycol (PEG)-protected gold nanorods (PEG-GNRs)	Axial sizes of 12.7 ± 3.4 and 47 ± 9.3 nm	–	Photothermal therapy in vitro and in vivo	[113]
Dumbbel-shaped Au-Fe_3O_4 nanoparticles	32 nm	Anti-HER2 (Herceptin) antibody	Drug delivery (platin complex) in vitro	[114]
Polyethylene glycol (PEG)-coated gold nanoparticles (PEG-AuNPs)	17.0 ± 2.0 nm	–	Drug delivery [doxorubicin (DOX)] in vitro	[116]
Poly(allylamine hydrochloride) (PAH), PEI and poly(diallyl dimethyl ammonium chloride) (PDDA) modified gold nanoparticles	11.8 ± 0.9 nm	–	Gene delivery (EGFR siRNA) in vitro	[119]
Gold nanoparticles (GNPs)	2–16 nm	–	Gene delivery [specific oligonucleotide sequence (POY2T)] in vitro	[120]
Gold nanospheres	5 nm	Nucleolin-target aptamer (AS1411)	Gene delivery in vitro and in vivo	[121]
Gold nanoparticles (GNPs)	–	Nucleolin-target aptamer (AS1411)	Gene (AZD8055) and drug delivery [doxorubicin (Dox)] in vitro	[122]
Spherical gold nanoparticles functionalized with BSA	100 nm	Folic acid (FA)	Drug co-delivery [methotrexate (MTX) and anti-TGF-β1 antibody] in vitro	[123]
Mercaptosuccinic acid (MSA)-capped gold nanoconstructs	32–41 nm	–	Drug co-delivery [SMI#9 (Rad6 protein inhibitor) and cisplatin] in vitro	[124]
Gold nanorods (GNRs)	–	Folic acid (FA)	Photothermal therapy (PTT) and drug delivery (cisplatin) in vivo	[125]
Gold nanorods (GNRs)	160.9–250 nm	–	NIR imaging and drug delivery [doxorubicin (DOC)] in vitro and in vivo	[126]
Gold nanorods (GNRs)	–	–	Photothermal ablation, gene (DNA) and drug [doxorubicin (DOX)] delivery in vivo	[127]
Gold nanospheres	40 nm (1.7 microg DOX/ microg Au)		Photothermal ablation and drug [doxorubicin (DOX)] delivery in vitro	[128]

The photothermal effect of gold nanocages (GNCs) conjugated with monoclonal antibodies (anti-HER2) to target breast cancer cells (SK-BR-3) was recently reported [103, 104]. The study showed that the nanocages strongly absorbed light in the NIR region to induce thermal destruction of the cancer cells.

Anti-HER2-conjugated gold nanoshells (GNShs) were reported as theranostic agents that accumulated in high

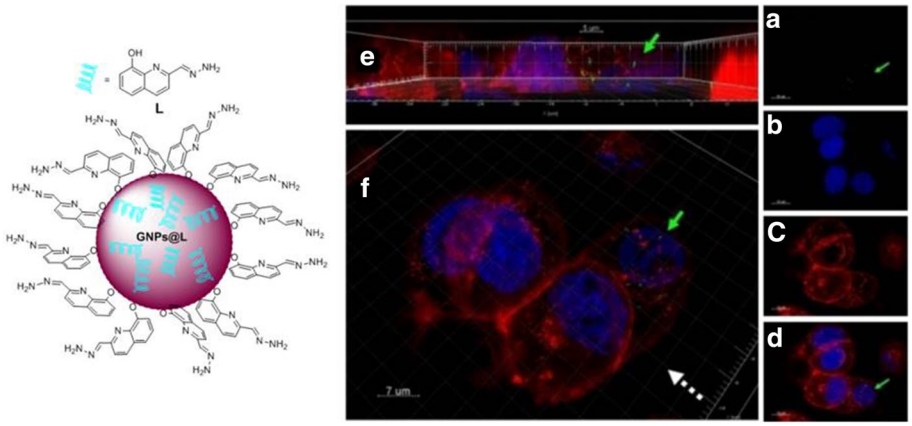

Fig. 2 Left schematic representation of the quinoline-based fluorescent sensor L and gold nanoparticles coated with compound L (GNPs@L). Right MCF-7 cells were exposed to GNPs@L (15 µg/ml) for 3 h before in vitro imaging. Confocal images of MCF-7 treated cells show clusters of gold nanoparticles accumulated in the cytoplasm (green arrows). Images were obtained as single channels of nanoparticle reflection (**a**), nuclear stain with Hoechst (**b**) and membrane stain with CellMask red (**c**). Merge image of all individual channels (**d**), 3D reconstruction (**f**) and Z projection (**e**), were generated using Bitplane Imaris 7.2.1 software (Reprinted (adapted) with permission from [24]. Copyright (2014) Elsevier)

concentration in breast cancer cells and also as a promising treatment option for chemotherapy resistant cancers [105]. In this way, Carpin et al. [106] demonstrated that anti-HER2-conjugated silica-gold nanoshells can mediate the effective targeting and photothermal ablation of two HER2-expressing breast cancer cell lines, which are both resistant to treatment with trastuzumab.

Gold nanostars (GNSs) showed unique plasmon properties that efficiently transduce photon energy into heat for PTT [107]. Using SKBR3 breast cancer cells incubated with bare GNSs, Yuan et al. demonstrated the photothermal ablation within 5 min of irradiation (980 nm continuous-wave laser 15 W/cm^2) [108]. On a mouse injected systemically with PEGylated GNSs for 2 days, extravasation of nanostars was observed and localized photothermal ablation was reported on a dorsal window chamber within 10 min of irradiation (785 nm continuous-wave laser 1.1 W/cm^2).

Similarly, Yuan et al. prepared [109] TAT-peptide functionalized GNSs for both enhanced intracellular particle delivery and efficient in vitro photothermolysis using an NIR femtosecond laser under an irradiance of 0.2 W/cm^2. After the incubation of TAT-GNS with BT549 breast cancer cells (4 h), photothermolysis was accomplished. It was observed that the enhanced intracellular delivery of TAT-GNS substantially potentiated the photothermolysis efficiency without compromising cell viability. GNSs showed an extremely strong two-photon photoluminescence (TPL) process.

Gold nanorods (GNRs) have a high surface area and are biocompatible, hence, a promising approach for breast cancer [110, 111]. Besides nanoshells, efforts were also made to use nanorods in PTT [112]. von Maltzahn et al. [113] synthesized polyethylene glycol (PEG)-protected gold nanorods (PEG-GNRs) that exhibited better spectral bandwidth and photothermal heat generation than gold–silica nanoshells, showing great potential for ultraselective tumor ablation. They found that PEG-GNRs rapidly generated more than 6 times of heat generated by PEG-gold nanoshells under identical experimental conditions, and can cause more efficient destruction of human tumor cells (MDA-MB-435) after light irradiation. In vivo study showed that intravenous injection of PEG-GNRs enabled the destruction of human xenograft tumors in mice upon irradiation.

Gold nanoparticles have also exhibited unique chemical and physical properties for transporting and unloading the pharmaceuticals. They are essentially inert, non-toxic, and in the size range of 1 nm to 150 nm. Moreover, they can be functionalized and modified to improve the versatility of gold nanoparticles. Significant efforts have been devoted over the past years to the fabrication of gold nanoparticles for the delivery of anticancer drugs.

In this way, dumbbel-shaped Au-Fe_3O_4 nanoparticles (NPs) have been made and coupled with Herceptin and a platin complex. The platin-Au-Fe_3O_4-Herceptin NPs act as a target-specific nanocarrier for delivery of platin into Her2-positive breast cancer cells (Sk-Br3) with strong therapeutic effects. The conjugate has a half-maximal inhibitory concentration (IC_{50}) toward Sk-Br3 cells [114].

Furthermore, multidrug resistance (MDR) has been a major impediment to the success of cancer chemotherapy and interest is growing in the development of drug delivery systems using nanotechnology to reverse MDR in cancer [115]. Through the development of a drug delivery system that tethers doxorubicin onto the surface of gold nanoparticles with a poly(ethylene glycol) spacer via an acid-labile

linkage (DOXHyd@ AuNPs), Wang et al. [116] demonstrated that multidrug resistance in cancer cells can be significantly overcome by a combination of a responsive intracellular release of doxorubicin from the gold nanoparticles in acidic organelles and a highly efficient cellular entry. They have also shown that such a delivery system can significantly inhibit the growth of multidrug-resistant MCF-7/ADR cancer cells, owing to the high efficiency of cellular uptake by endocytosis and subsequent acid responsive release in cells.

It has been reported that the conjugation of nucleic acids with gold nanoparticles leads to an increase of nucleic acids stability and prevents their degradation by cellular enzymes [117, 118]. In order to construct siRNA delivery systems, poly(allylamine hydrochloride) (PAH), PEI and poly(diallyl dimethyl ammonium chloride) (PDDA), and siRNA were assembled on the surface of gold nanoparticles, respectively, by the ionic layer-by-layer method. After stabilization with denatured bovine serum albumin, the EGFR siRNA delivered by PAH-modified gold nanoparticles exhibited an improved silencing effect when compared to Lipofectamine 2000® [119].

It was found that gold nanoparticles loaded with a specific oligonucleotide sequence (POY2T) were able to enter into the nucleus of breast carcinoma cell lines and inhibit cell proliferation by regulating the expression of the c-myc gene (decreased by 40% in MCF-7 breast cancer cells) that plays a key role in the carcinogenesis process [120].

Additionally, gold nanospheres functionalized with a nucleolin-target aptamer (AS1411) had an intense antiproliferative effect specifically on breast cancer cell lines [MDA-MB-231 (88%) and MCF-7(80%)] in a concentration about 20-fold less than that needed using the aptamer alone. A complete inhibition of tumor growth and tumor regression was observed after systemic administration of AS1411-gold in MDA-MB-231 xenografts mouse models [121]. Similarly, the surface modification of gold nanoparticles with the AS1411 aptamer led to a high affinity to the nucleolin overexpressed on the surface of malignant cells in vitro, providing an increased specificity and targeted delivery of doxorubicin (Dox) towards malignant cells, including MCF-7 breast cancer cells [122]. Due to its high specificity, the AS1411-Dox-gold nanosystem increased breast cancer cell death by about 50% compared to Dox-gold nanoparticles modified with a nonspecific aptamer.

Synergistic treatment with different anticancer agents using nanoplatforms has been provided superior anti-tumor effects in preclinical studies. In this way, spherical gold nanoparticles functionalized with folic acid-BSA and combining two different anti-cancer drugs (methotrexate and anti-TGF-β1 antibody) were used for combinational therapy in metastatic breast cancer cells overexpressing TGF-β1 protein [123]. It was found that the levels of free extracellular TGF-β1, associated with cancer progression and metastasis, were reduced by 30% in cells exposed to targeted nanoparticles compared to unexposed cells and by 10% compared to free anti-TGF-β1 antibody.

A significant enhancement in triple negative breast cancer cells sensitivity to the cisplatin drug was observed when the treatment was combined with the exposure to mercaptosuccinic acid (MSA)-capped gold nanoconstructs loaded with SMI#9 (Rad6 protein inhibitor). The effective dose of cisplatin needed to inhibit the growth of 50% of cancer cells (4.9 μM) was at least 5 times less than in the treatment with free cisplatin (> 25 μM) in vitro [124] which may lead to a more tolerable treatment for patients in a still efficacious dose.

As an example of multi-modal therapy, a single platform composed of folic acid-targeted nanoparticles carrying cisplatin drug were developed [125]. This nanoprobe showed high accumulation into tumors and a synergistic effect in vivo to kill orthotopic triple negative breast tumors combined with photothermal therapy (PTT), which lead to virtually complete tumor eradication. No tumor growth was detected at day 20 post-administration of folic acid-cisplatin-gold nanorods followed by irradiation, significantly different from the growth rates (tumor volume > 600 mm^3) observed in tumors treated in other conditions. Additionally, the cotreatment suppressed the breast cancer metastasis to the lung by disrupting the peripheral tumor vasculature.

A NIR light-sensitive targeted nanoparticles based on gold nanorods loaded with doxorubicin demonstrated a significant in vivo anticancer activity showing its potential for synergistic therapy in breast cancer treatment. Moreover, the encapsulation of doxorubicin in the nanosystem reduced significantly the systemic toxicity caused by the free drug [126].

To treat metastatic breast cancer, a Dox-loaded DNA-wrapped gold nanorod was developed, which allowed for dual therapeutic functions, photothermal ablation and, chemotherapy [127]. Mice bearing 4T1 mammary tumors were treated with the Dox-loaded DNA-wrapped gold nanorod and received 655-nm laser irradiation. A significant reduction of primary tumor growth was observed in the gold nanorod-treated mice as well as a suppression in lung metastases when compared with untreated mice [127].

Another hollow gold nanosphere, which is a promising theranostic nanoparticle platform, has plasmon absorption in the NIR region and displays strong photothermal coupling properties suitable for photothermal ablation therapy [128]. The hollow gold nanospheres (HAuNS, ~ 40-nm diameter) could carry large amounts of Dox (63% by weight), and drug release can be triggered by NIR light irradiation. The dual therapeutic effects of Dox-loaded HAuNS and laser irradiation were demonstrated through enhanced cell death of combination treated groups compared with single treatment groups in the human TNBC MDA-MB-231 cell line [128].

Future perspectives

Imaging has an essential role in breast cancer detection. Mammographic screening reduces breast cancer mortality, however, despite high sensitivity of radiological screening, the specificity of breast radiological imaging has been demonstrated as low as 71%.

Nanotechnology offers the possibility of significantly improving radiological screening methods. Owing to their significant advantages over traditional contrast agents, superparamagnetic NPs were used as an alternative to conventional radiological agents. Additionally, studies have shown that the iron released from degrading SPIONs is metabolized by the body, reducing the potential for long-term cytotoxicity.

The use of dual-modality nanoprobes to detect or analyze cells, (optical and MRI) could improve the diagnostic quality of breast tumors. MR imaging can offer high spatial resolution and the capacity to simultaneously obtain physiological and anatomical information, whereas optical imaging allows for high sensitivity and provides the real-time molecular targeting of images.

Furthermore, nanoparticles with MRI and fluorescence imaging (FI) dual-modality are able to label and track targeting cells in tissue or solid tumors. To this aim, SPIONs are generally combined with either fluorescent dyes or quantum dots (e.g. CdSe/ZnS) and used as bimodal magnetic-fluorescent nanoprobes for cell labeling and MRI applications. QDs have excellent optical properties; therefore, they have great potential to be applied in tumor imaging field as fluorescence probes in vivo. Although QD probes have their own advantages, it also has some drawbacks. The wavelength of emission photon of QD was coincidence with the emission band of tissue autofluorescence in the visible range. Furthermore, the fluorescence of QD shows low spatial resolution in organ analysis. These disadvantages can effectively be compensated by the magnetic resonance imaging (MRI).

The discovery and characterization of novel breast cancer markers will usher in new targeting moieties. In this way, researchers have been conjugating inorganic nanoparticles (superparamagnetic, quantum dots and gold nanoparticles) with various ligands and biomolecules to develop strategies for targeted delivery.

Combinational therapies using multifunctional nanoplatforms to fight cancer have acquired special attention in the recent years. The combination of two or more anticancer agents or the combination of more than one therapeutic approach (multi-modal therapy) can synergistically improve treatment efficacy and decrease tumor drug resistance with reduced side effects.

Acknowledgements Authors thank "Instituto de Salud Carlos III" (Plan Estatal de I+D+i 2013–2016 and European Regional Development Fund) of the Spanish Ministry of Economy and Competitiveness. C. Núñez acknowledges her personal Miguel Servet Contract (CP16/00139).

References

1. Siegel RL, Miller K, Jemal AJ (2016) CA Cancer J Clin 65:7–30
2. Kunnath AP, Tiash S, Fatemian T, Morshed M, Mohamed SM, Chowdhury EH (2014) J Cancer Sci Ther 6(4):099–104
3. Geiser WR, Haygood TM, Santiago L, Stephens T, Thames D, Whitman GJ (2011) AJR Am J Roentgenol 197:W1023–W1030
4. Astley SM (2004) Br J Radiol 77:S194–S200
5. Veronesi U, Boyle P, Goldhirsch A, Orecchia R, Viale G (2005) Breast cancer. Lancet 365:1727–1741
6. Dixon JM, Anderson TJ, Page DL, Lee D, Duffy SW (1982) Histopathology 6:149–161
7. Collett K, Stefansson IM, Eide J, Braaten A, Wang H, Eide GE, Thoresen SO, Foulkes WD, Akslen LA (2005) Cancer Epidemiol Biomark Prev 14:1108–1112
8. Silverstein MJ, Lewinsky BS, Waisman JR, Gierson ED, Colburn WJ, Senofsky GM, Gamagami P (1994) Cancer 73:1673–1677
9. Porter PL, El-Bastawissi AY, Mandelson MT, Lin MG, Khalid N, Watney EA, Cousens L, White D, Taplin S, White E (1999) J Natl Cancer Inst 91:2020–2028
10. Brigger I, Dubernet C, Couvreur P (2012) Adv Drug Deliv Rev 54:631–651
11. Choi Y-E, Kwak J-W, Park JW (2010) Sensors 10:428–455
12. Conde J, Doria G, Baptista P (2012) J Drug Deliv 2012:751075
13. Park JW (2002) Breast Cancer Res 4(3):95–99
14. Lee CC, MacKay JA, Frechet JM, Szoka FC (2005) Nat Biotechnol 23(12):1517–1526
15. Yezhelyev M, Yacoub R, O'Regan R (2009) Nanomedicine 4(1):83–103
16. Lidke DS, Nagy P, Heintzmann R, Arndt-Jovin DJ, Post JN, Grecco HE, Jares-Erijman EA, Jovin TM (2004) Nat Biotechnol 22:198–203
17. Oliveira E, Núñez C, Rodríguez-González B, Capelo JL, Lodeiro C (2011) Inorg Chem 50(18):8797–8807
18. Fernández-Lodeiro J, Núñez C, Oliveira E, Capelo JL, Lodeiro C (2013) J Nanopart Res 15(8):1828–1838
19. Fernández-Lodeiro A, Fernández-Lodeiro J, Núñez C, Bastida R, Capelo JL, Lodeiro C (2013) ChemistryOpen 2(56):200–207
20. Fernández-Lodeiro J, Núñez C, Fernández-Lodeiro A, Oliveira E, Rodríguez-González B, Dos Santos AA, Capelo JL, Lodeiro C (2014) J Nanopart Res 16:2315–2317
21. Oliveira E, Núñez C, Santos HM, Fernández-Lodeiro J, Fernández-Lodeiro A, Capelo JL, Lodeiro C (2015) Sens Actuators B Chem 212:297–328
22. Fernández-Lodeiro A, Fernández-Lodeiro J, Núñez C, Oliveira E, Santos HM, Lodeiro C, Capelo JL, Diniz MS (2013) Microsc Microanal 19:25–26
23. López-Cortés R, Oliveira E, Núñez C, Lodeiro C, de la Cadena MP, Fernández-Riverola F, López-Fernández H, Reboiro-Jato M, González-Peña D, Capelo JL, Santos HM (2012) Talanta 100:239–245
24. Núñez C, Oliveira E, García-Pardo J, Diniz M, Lorenzo J, Capelo JL, Lodeiro C (2014) J Inorg Biochem 137:115–122
25. Núñez C, Capelo JL, Igrejas G, Alfonso A, Botana LM, Lodeiro C (2016) Biomaterials 97:34–50
26. Saadeh Y, Leung T, Vyas A, Chaturvedi LS, Perumal O, Vyas D (2014) J Nanosci Nanotechnol 14:913–923
27. Stark DD, Weissleder R, Elizondo G (1998) Radiology 168(2):297–301

28. Hong RY, Li JH, Qu JM, Chen LL, Li HZ (2009) Chem Eng J 150:572–580
29. Kim DK, Mikhaylova M, Wang FH, Kehr J, Bjelke B, Zhang Y, Tsakalakos T, Muhammed M (2003) Chem Mater 15:4343–4351
30. Ma HL, Xu YF, Qi XR, Maitani Y, Nagai T (2008) Int J Pharm 354:217–226
31. Cheng F, Wang SP, Su C, Tsai T, Wu P, Shieh D, Chen J, Hsieh PC, Yeh C (2008) Biomaterials 29:2104–2112
32. Gupta AK, Curtis ASG (2004) J Mater Sci Mater Med 15:493–496
33. Lu AH, Salabas EL, Schuth F (2007) Angew Chem Int Ed Engl 46(8):1222–1244
34. Thorek DL, Chen AK, Czupryna J, Tsourkas A (2006) Ann Biomed Eng 34(1):23–38
35. Scherer F, Anton M, Schillinger U, Henke J, Bergemann C, Krüger A, Gänsbacher B, Plank C (2002) Gene Ther 9(2):102–109
36. Okarvi SM, Al Jammaz I (2010) Nucl Med Biol 37:277–288
37. Chanda N, Kattumuri V, Shukla R, Zambre A, Katti K, Upendran A, Kulkarni RR, Kan P, Fent GM, Casteel SW, Smith CJ, Boote E, Robertson JD, Cutler C, Lever JR, Katti KV, Kannana R (2010) PNAS 107:8760–8765
38. Jafari A, Salouti M, Shayesteh SF, Heidari Z, Rajabi AB, Boustani K, Nahardani A (2015) Nanotechnology 26:075101
39. Zhang C, Jugold M, Woenne EC, Lammers T, Morgenstern B, Mueller MM, Zentgraf H, Bock M, Eisenhut M, Semmler W, Kiessling F (2007) Cancer Res 67:1555–1562
40. Gong F, Zhang Z, Chen X, Zhang L, Yu X, Yang Q, Shuai X, Liang B (2014) Chin J Polym Sci 32:321–332
41. Yan C, Wu Y, Feng J, Chen W, Liu X, Hao P, Yang R, Zhang J, Lin B, Xu Y, Liu R (2013) Int J Nanomed 8:245–255
42. Kresse M, Wagner S, Pfefferer D, Lawaczeck R, Elste V, Semmler W (1998) Magn Reson Med 40:236–242
43. Chen T-J, Cheng T-H, Chen C-Y, Hsu SC, Cheng T-L, Liu G-C, Wang YM (2009) J Biol Inorg Chem 14:253–260
44. Huh Y-M, Jun Y-W, Song H-T, Kim S, Choi J-S, Lee J-H, Yoon S, Kim K-S, Shin J-S, Suh J-S, Cheon J (2005) J Am Chem Soc 127:12387–12391
45. Kievit FM, Stephen ZR, Veiseh O, Arami H, Wang T, Lai VP, Park JO, Ellenbogen RG, Disis ML, Zhang M (2012) ACS Nano 6:2591–2601
46. Zhang J, Dewilde AH, Chinn P, Foreman A, Barry S, Kanne D, Braunhut SJ (2011) Int J Hyperth 27:682–697
47. Mu Q, Kievit FM, Kant RJ, Lin G, Jeon M, Zhang M (2015) Nanoscale 7:18010–18014
48. Bae KH, Lee K, Kim C, Park TG (2011) Biomaterials 32:176–184
49. Aires A, Ocampo SM, Simões BM, Rodríguez MJ, Cadenas JF, Couleaud P, Spence K, Latorre A, Miranda R, Somoza Á, Al E (2016) Nanotechnology 27:65103
50. Sun C, Sze R, Zhang M (2006) J Biomed Mater Res 78:550–557
51. Yang H, Zhuang YM, Hu H, Du XX, Zhang CX, Shi XY, Wu HX, Yang SP (2010) Adv Funct Mater 20:1733–1741
52. Akal ZÜ, Alpsoy L, Baykal A (2016) Ceram Int 42:9065–9072
53. Akal ZÜ, Alpsoy L, Baykal A (2016) Appl Surf Sci 378:572–581
54. Yang L, Cao Z, Sajja HK, Mao H, Wang L, Geng H, Xu H, Jiang T, Wood WC, Nie S, Wang YA (2008) J Biomed Nanotechnol 4:439–449
55. Cao Z, Lee GY, Wang A, Sajja HK, Wang L, Long R, Barwick BG, Leyland-Jones BR, Wood WC, Nie S, Mao H, Yang L (2010) Cancer Res 70:5482
56. Gao GH, Heo H, Lee JH, Lee DS (2010) J Mater Chem 20:5454–5461
57. Li JJ, You J, Dai Y, Shi ML, Han CP, Xu K (2014) Anal Chem 86:11306–11311
58. Kohler N, Sun C, Wang J, Zhang M (2005) Langmuir 21:8858–8864
59. Sun Y, Zheng Y, Ran H, Zhou Y, Shen H, Chen Y, Chen H, Krupka TM, Li A, Li P, Wang Z, Wang Z (2012) Biomaterials 33:5854–5864
60. Shiozawa M, Kobayashi S, Sato Y, Maeshima H, Hozumi Y, Lefor AT, Kurihara K, Sata N, Yasuda Y (2014) Breast Cancer 21:394–401
61. Nakai G, Matsuki M, Harada T, Tanigawa N, Yamada T, Barentsz J, Narumi Y (2011) J Magn Reson Imaging 34:557–562
62. Shan XH, Wang P, Xiong F, Gu N, Hu H, Qian W, Lu HY, Fan Y (2016) Mol Imaging Biol 18:24–33
63. Chiang C-S, Hu S-H, Liao B-J, Chang Y-C, Chen S-Y (2014) Nanomedicine 10:99–107
64. Lee JY, Kim J-H, Bae KH, Oh MH, Kim Y, Kim JS, Park TG, Park K, Lee JH, Nam YS (2015) Small 11:222–231
65. Medintz IL, Uyeda HT, Goldman ER, Mattoussi H (2005) Nat Mater 4(6):435–446
66. Gao X, Cui Y, Levenson RM, Chung LWK, Nie S (2004) Nat Biotechnol 22(8):969–976
67. Chan WC, Nie S (1998) Science 281(5385):2016–2018
68. Wang L-W, Peng C-W, Chen C, Li Y (2015) Breast Cancer Res Treat 151(1):7–17
69. Seifalian A, Rizvi S, Rouhi S, Taniguchi S, Yang SY, Green M, Keshtgar M, Seifalian AM (2014) Int J Nanomed 9:1323–1337
70. Tada H, Higuchi H, Wanatabe TM, Ohuchi N (2007) Cancer Res 67:1138–1144
71. Chen C, Peng J, Xia HS, Yang GF, Wu QS, Chen LD, Zeng LB, Zhang ZL, Pang DW, Li Y (2009) Biomaterials 30:2912–2918
72. Balalaeva IV, Zdobnova TA, Krutova IV, Brilkina AA, Lebedenko EN, Deyev SM (2012) J Biophotonics 5:860–867
73. Chen C, Peng J, Sun SR, Peng CW, Li Y, Pang DW (2012) Nanomedicine (Lond) 7:411–428
74. Chen C, Peng J, Xia H, Wu Q, Zeng L, Xu H, Tang H, Zhang Z, Zhu X, Pang D, Li Y (2010) Nanotechnology 21:095101
75. Liu X-L, Peng C-W, Chen C, Yang X-Q, Hu M-B, Xi H-S, Liu S-P, Pang D-W, Li Y (2011) Biochem Biophys Res Commun 409:577–582
76. Yezhelyev MV, Al-Hajj A, Morris C, Marcus AI, Liu T, Lewis M, Cohen C, Zrazhevskiy P, Simons JW, Rogatko A, Nie S, Gao X, O'Regan RM (2007) Adv Mater 19:3146–3151
77. Wu XY, Liu HJ, Liu JQ, Haley KN, Treadway JA, Larson JP, Ge N, Peale F, Bruchez MP (2003) Nat Biotechnol 21:41–46
78. Tan YF, Chandrasekharan P, Maity D, Yong CX, Chuang K-H, Zhao Y, Wang S, Ding J, Feng S-S (2011) Biomaterials 32:2969–2978
79. Ma Q, Nakane Y, Mori Y, Hasegawa M, Yoshioka Y, Watanabe TM, Gonda K, Ohuchi N, Jin T (2012) Biomaterials 33:8486–8494
80. Park JH, von Maltzahn G, Ruoslahti E, Bhatia SN, Sailor MJ (2008) Angew Chem Int Ed Engl 47:7284–7288
81. Takeda M, Tada H, Higuchi H, Kobayashi Y, Kobayashi M, Sakurai Y, Ishida T, Ohuchi N (2008) Breast Cancer 15:145–152
82. Alibolandi M, Abnous K, Sadeghi F, Hosseinkhani H, Ramezani M, Hadizadeh F (2016) Int J Pharm 500(1–2):162–178
83. Tan WB, Jiang S, Zhang Y (2007) Biomaterials 28:1565–1571
84. Yezhelyev MV, Qi L, O'Regan RM, Nie S, Gao X (2008) J Am Chem Soc 130:9006–9012
85. Li Y, Li Z, Wang X, Liu F, Cheng Y, Zhang B, Shi D (2012) Theranostics 2:769–776
86. Ntziachristos V, Bremer C, Weissleder R (2003) Eur Radiol 13:195–208
87. SalmanOgli A, Rostami A (2012) IEEE Trans Nanotechnol 11:1183–1191
88. Daniel MC, Astruc D (2004) Chem Rev 104(1):293–346

89. Paciotti GF, Myer L, Weinreich D, Goia D, Pavel N, McLaughlin RE, Tamarkin L (2004) Drug Deliv 11(3):169–183
90. El-Sayed IH, Huang X, El-Sayed MA (2006) Cancer Lett 239(1):129–135
91. Agasti SS, Rana S, Park MH, Kim CK, You CC, Rotello VM (2010) Adv Drug Deliv Rev 62:316–328
92. Hahn MA, Singh AK, Sharma P, Brown SC, Moudgil BM (2011) Anal Bioanal Chem 399:3–27
93. Di Pasqua AJ, Mishler RE II, Ship YL, Dabrowiak JC, Asefa T (2009) Mater Lett 63:1876–1879
94. Elmes RBP, Orange KN, Cloonan SM, Williams DC, Gunnlaugsson T (2011) J Am Chem Soc 133:15862–15865
95. Martínez-Calvo M, Orange KN, Elmes RBP, Poulsen B, Williams DC, Gunnlaugsson T (2016) Nanoscale 8:563–574
96. Tonga GY, Jeong Y, Duncan B, Mizuhara T, Mout R, Das R, Kim ST, Yeh Y, Yan B, Hou S, Rotello VM (2015) Nat Chem 7:597–603
97. Rayavarrapu RG, Peterson W, Ungureanu C, Post JN, van Leeuwen TG, Manohar S (2007) Int J Biomed Imaging 2007:29817
98. Eghtedari M, Liopo AV, Copland JA, Oraevsky AA, Motamed M (2009) Nano Lett 9:287–291
99. Nie L, Wang S, Wang X, Rong P, Ma Y, Liu G, Huang P, Lu G, Chen X (2014) Small 10:1585–1593
100. Galanzha EI, Shashkov EV, Kelly T, Kim J-W, Yang L, Zharov VP (2009) Nat Nanotechnol 4:855–860
101. Bednarz-Knoll N, Alix-Panabières C, Pantel K (2011) Breast Cancer Res 13:228
102. Abadeer NS, Murphy CJ (2016) J Phys Chem C 120:4691–4716
103. Chen J, Wang D, Xi J, Au L, Siekkinen A, Warsen A, Li ZY, Zhang H, Xia Y, Li X (2007) Nano Lett 7:1318–1322
104. Au L, Zheng D, Zhou F, Li ZY, Li X, Xia Y (2008) ACS Nano 2:1645–1652
105. Morton JG, Day ES, Halas NJ, West JL (2010) Methods Mol Biol 624:101–117
106. Carpin LB, Bickford LR, Agollah G, Yu T-K, Schiff R, Li Y, Drezek RA (2011) Breast Cancer Res Treat 125:27–34
107. Guerrero-Martínez A, Barbosa S, Pastoriza-Santos I, Liz-Marzán LM (2011) Curr Opin Colloid Interface Sci 16:118–127
108. Yuan H, Khoury CG, Wilson CM, Grant GA, Bennett AJ, Vo-Dinh T (2012) Nanomedicine 8:1355–1363
109. Yuan H, Fales AM, Vo-Dinh T (2012) J Am Chem Soc 134:11358–11361
110. Tong L, Wei Q, Wei A, Cheng J-X (2009) Photochem Photobiol 85:21–32
111. Parab HJ, Chen HM, Lai T-C, Huang JH, Chen PH, Liu R-S, Hsiao M, Chen C-H, Tsai D-P, Hwu Y-K (2009) J Phys Chem C 113:7574–7578
112. Gobin AM, Watkins EM, Quevedo E, Colvin VL, West L (2011) Small 6:745–752
113. von Maltzahn G, Park J-H, Agrawal A, Bandaru NK, Das SK, Sailor MJ, Bhatia SN (2009) Cancer Res 69:3892–3900
114. Xu C, Wang B, Sun S (2009) J Am Chem Soc 131(12):4216–4217
115. Dong XW, Mumper RJ (2010) Nanomedicine (Lond.) 5:597–651
116. Wang F, Wang Y-C, Dou S, Xiong M-H, Sun T-M, Wang J (2011) ACS Nano 5:3679–3692
117. Han G, Martin CT, Rotello VM (2006) Chem Biol Drug Des 67:78–82
118. Seferos DS, Prigodich AE, Giljohann DA, Patel PC, Mirkin CA (2009) Nano Lett 9:308–311
119. Zhao E, Zhao Z, Wang J, Yang C, Chen C, Gao L, Feng Q, Hou W, Gao M, Zhang Q (2012) Nanoscale 4:5102–5109
120. Huo S, Jin S, Ma X, Xue X, Yang K, Kumar A, Wang PC, Zhang J, Hu Z, Liang XJ (2014) ACS Nano 8:5852–5862
121. Malik MT, O'toole MG, Casson LK, Thomas SD, Bardi GT, Reyes-Reyes EM, Ng CK, Kang KA, Bates PJ (2015) Oncotarget 6:22270–22281
122. Latorre A, Posch C, Garcimartín Y, Celli A, Sanlorenzo M, Vujic I, Ma J, Zekhtser M, Rappersberger K, Ortiz-Urda S, Somoza Á (2014) Nanoscale 6:7436–7442
123. Rizk N, Christoforou N, Lee S (2016) Nanotechnology 27:185704
124. Haynes B, Zhang Y, Liu F, Li J, Petit S, Kothayer H, Bao X, Westwell AD, Mao G, Shekhar MPV (2016) Nanomedicine 12:745–757
125. Feng B, Xu Z, Zhou F, Yu H, Sun Q, Wang D, Tang Z, Yu H, Yin Q, Zhang Z, Li Y (2015) Nanoscale 7:14854–14864
126. Liang Y, Gao W, Peng X, Deng X, Sun C, Wu H, He B (2016) Biomaterials 100:76–90
127. Wang D, Xu Z, Yu H, Chen X, Feng B, Cui Z, Lin B, Yin Q, Zhang Z, Chen C, Wang J, Zhang W, Li Y (2014) Biomaterials 35:8374–8384
128. You J, Zhang G, Li C (2010) ACS Nano 4:1033–1041